FI SEVIER

Contents lists available at ScienceDirect

# **Optics Communications**

journal homepage: www.elsevier.com/locate/optcom



# Field-compensated birefringent Fourier transform spectrometer

Jie Li, Jingping Zhu\*, Xun Hou

Key Laboratory for Physical Electronics and Devices of the Ministry of Education and Shaanxi Key Lab of Information Photonic Technique, Xi'an Jiaotong University, Xi'an 710049, PR China

## ARTICLE INFO

Article history: Received 10 July 2010 Received in revised form 5 November 2010 Accepted 11 November 2010

Keywords:
Birefringent Fourier transform spectrometer
Field compensation
High optical throughput

#### ABSTRACT

A field-compensation method applied for Savart birefringent Fourier transform spectrometer is presented. By using a combination of Savart plates fabricated from positive and negative birefringent materials, the useful solid angle of field of view can be increased by a large amount in broad spectral coverage. Compared to the conventional Fourier transform spectrometers, the compensated field angle has optical throughput higher by one order in magnitude. To demonstrate the effectiveness, a design example operating at 400–1100 nm with a large solid angle exceeding  $\pm$  40° is presented in detail.

© 2010 Elsevier B.V. All rights reserved.

#### 1. Introduction

Fourier transform spectrometers (FTSs) have huge potential in a wide variety of applications, such as chemistry, biomedicine, agriculture, astronomy and remote sensing [1,2]. A FTS offers many advantages over other forms of spectroscopic measurement. Most prominent among these is the Jacquinot (high optical throughput) advantage. At the same resolutions, the optical throughput of a FTS based on a Michelson interferometer is almost 200 times greater than that of a dispersive spectrometer [3]. High optical throughput increases the instrument sensitivity and allows the recording of high resolution spectra at low light levels.

However, in a FTS based on Michelson interferometer, precision scanning mechanisms and highly stable designs are usually essential for the spectra measurement of light, especially in the UV and visible regions. This implies high cost, complexity and substantial bulk. To solve these problems, a number of compact and robust designs have been proposed that produce interferograms with no moving parts, such as Sagnac-based [4,5], Wollaston prisms based [6–9] and Savart polariscope based [10,11] FTSs. The latter two are also always called birefringent FTS.

Nevertheless, the previous static designs did not exhibit the full extent of the Jacquinot advantage because of the limited field of view (FOV) of the instruments. The optical throughput E of a FTS is defined as  $E=\Omega A$ , where  $\Omega$  is the solid angle of the FOV for the spectrometer, A is the area of its input aperture. For a typical static FTS based on Wollaston prisms, the FOV is normally only about a third of the Michelson-based FTSs [6]. To overcome this shortcoming, several designs of Field-widened birefringent FTS have been reported.

Courtial et al. find that a  $\pm 15^\circ$  FOV can be obtained when an achromatic half-wave plate is included between two Wollaston prisms [12]. Boer et al. increase the FOV of a FTS based on Wollaston prism by more than  $\pm 35^\circ$  using liquid-crystal technology [13]. Françon et al. propose a more than  $\pm 10^\circ$  wide-angle FTS based on two Wollaston prisms made of different crystals of opposite signs, and demonstrate a modified Savart polariscope for large angle of incidence by using a half-wave plate to estimate the second term related to incidence angle in the optical path difference (OPD) [14]. Zhang et al. report their designs to increase FOV of a FTS based on combined Savart polariscopes with different optical axes up to  $\pm 14^\circ$  by cancelling the first term related to incidence angle in the OPD [15].

In this paper we propose an alternative field-compensated method to increase the accepted solid angle of a static birefringent FTS based on Savart plates. It is demonstrated that in a combination of two Savart polariscopes fabricated from positive and negative birefringent materials, the FOV of the described instrument can be increased much wider in an ultra broadband spectrum than that of any previous design. This in turn increases the optical throughput by one order of magnitude compared to that of a conventional Michelson-based FTS with the same resolution.

#### 2. Theory

The concept of a general static FTS is presented in Fig. 1. It consists of a collimator, a beamsplitter, an imaging lens and a linear detector array. The light to be measured is collected and collimated by the collimator and then resolved by the beamsplitter into two equal amplitude components that have a lateral displacement. Then the two coherent components are focused by the imaging lens to a common location at the linear detector array where they interfere. Compared with the FTS based on Michelson interferometer, the static FTS

<sup>\*</sup> Corresponding author. Tel./fax: +86 29 8266 8643 2732.

E-mail addresses: simon\_li139@163.com (J. Li), jpzhu@mail.xjtu.edu.cn (J. Zhu).

produces an interferogram in space on the detector array plane rather than in time according to the mirror scanning.

The key component in the static FTS is the beamsplitter and the maximum possible FOV of a static FTS is mainly determined by it. In order to show how two Savart polariscopes fabricated from materials with opposite signs of birefringence can increase FOV, we first briefly recall the previous designs of the Savart polariscopes.

## 2.1. Previous Savart polariscopes

A conventional Savart polariscope is made up of two identical uniaxial crystal plates cut at  $45^{\circ}$  to the optic axis and cemented together with their principle sections perpendicular to each other. As shown in Fig. 2, a Savart polariscope can be used as a polarization beamsplitter, introducing a lateral displacement between the two orthogonally polarized components (ordinary ray O and extraordinary ray E) of the incident light. When the Savart polariscope is placed between two polarizers and illuminated with white light, interference fringes can be obtained after the second polarizer. This is due to an OPD between the two polarization components that varies with the incidence angle of light.

The OPD produced by the first and second plates of the Savart polariscope can be given, respectively, by [16]

$$\begin{split} \Delta_1 &= t \bigg\{ \frac{1}{C} - \frac{1}{b} + \frac{\left(a^2 - b^2\right) \cos \omega}{2C^2} \sin i \\ &+ \frac{\sin^2 i}{2} \bigg[ \left(b - \frac{a^2}{C}\right) \sin^2 \omega + \left(b - \frac{a^2 b^2}{C^3}\right) \cos^2 \omega \bigg] \\ &+ \text{terms in } \sin^4 i, \text{etc.} \bigg\}, \end{split} \tag{1}$$

$$\Delta_{2} = t \left\{ \frac{1}{C} - \frac{1}{b} - \frac{\left(a^{2} - b^{2}\right)\sin\omega}{2C^{2}} \sin i + \frac{\sin^{2}i}{2} \left[ \left(b - \frac{a^{2}b^{2}}{C^{3}}\right)\sin^{2}\omega + \left(b - \frac{a^{2}}{C}\right)\cos^{2}\omega \right] + \text{terms in } \sin^{4}i, \text{etc.} \right\},$$

$$(2)$$

with  $a=1/n_e$ ,  $b=1/n_o$ , and  $C=[(a^2+b^2)/2]^{1/2}$ . Here  $n_e$  and  $n_o$  are crystal indexes for the extraordinary and ordinary component respectively; i is the incidence angle;  $\omega$  is the angle between the incidence plane and the principal section of the first Savart plate; t is

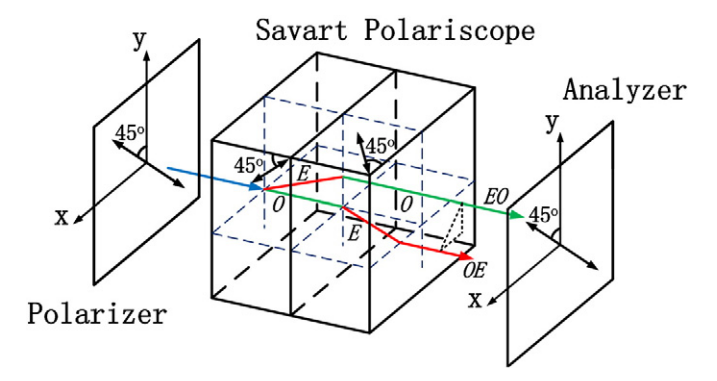


Fig. 2. Ray tracing of a Savart polariscope.

the thickness of a single Savart plate. Thus, the OPD introduced by the Savart polariscope can be expressed as [16]

$$\begin{split} \Delta_1 - \Delta_2 &= t \Big[ \frac{a^2 - b^2}{a^2 + b^2} (\cos \omega + \sin \omega) \sin i + \frac{a^2 - b^2}{\left(a^2 + b^2\right)^{3/2}} \\ &\quad \times \frac{a^2}{\sqrt{2}} \Big( \sin^2 \omega - \cos^2 \omega \Big) \sin^2 i + \text{terms in } \sin^4 i, \text{etc.} \Big]. \end{split} \tag{3}$$

Here the coefficient of the  $\sin i$  term is the lateral displacement produced by the Savart polariscope, and it can reach the maximum when  $\omega$  takes the value of 45°. It should be pointed out that a Savart polariscope produces fringes in the far field. Since the fringe pattern is detected on the focal plane of a lens following the polariscope, equal angles of incidence map the same line fringe in the detector arrays. In the center of the fringe pattern where the incidence angles are small, the  $\sin i$  term in Eq. (3) produces fringe patterns of constant spatial frequency. But in the margins where the incidence angles are large, the second and higher power terms of  $\sin i$  are not small anymore, and this will bring out hyperbolic fringes which is shown in Fig. 3. The angles of incidence are limited by this distortion. And the FOV can be defined usefully as the range of input angles i which obey the following  $\lambda/2$  condition [12] as

$$\Delta' = t \left[ \frac{a^2 - b^2}{\left(a^2 + b^2\right)^{3/2}} \cdot \frac{a^2}{\sqrt{2}} \left( \cos^2 \omega - \sin^2 \omega \right) \sin^2 i \right] \le \frac{\lambda}{2}, \tag{4}$$

where  $\lambda$  is the wavelength of the input light.

The fringe patterns produced by the conventional Savart polariscope above are not perfectly straight, even for small incidence angles. In order to obtain more nearly straight fringes and wider FOV, Françon [12] demonstrated a modified Savart polariscope which illustrated in

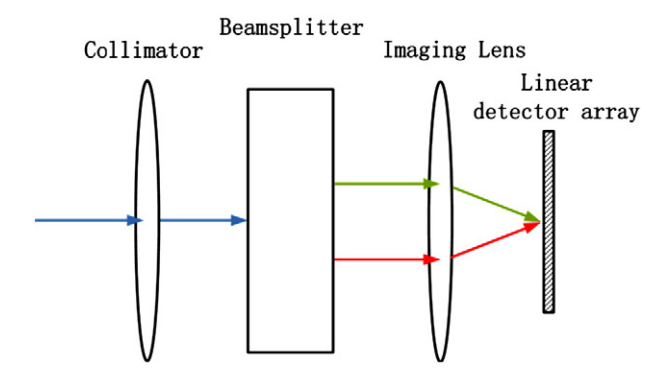


Fig. 1. General static FTS.

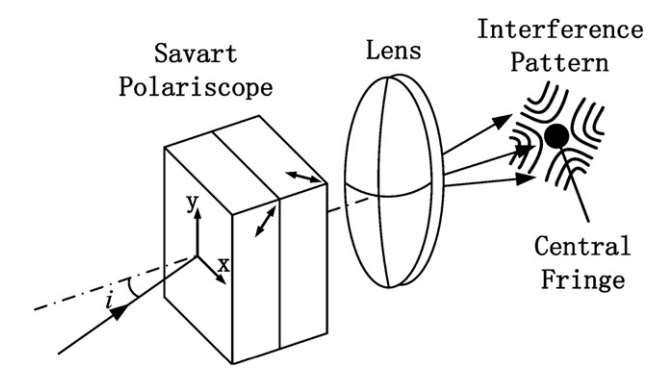


Fig. 3. Formation of interferogram fringes of a Savart polariscope in the fringe plane.

Fig. 4. With an exact rotation angle of the half-wave plate, the OPD of the modified Savart polariscope is given by

$$\Delta = 2t \frac{a^2 - b^2}{a^2 + b^2} \cos \omega \sin i. \tag{5}$$

There is no term in  $\sin^2 i$ ; the  $\sin^4 i$  term is almost always negligible. The FOV to acquire straight interference fringes can be very large theoretically. However, since the rotation angle of a half-wave plate is variable with the incidence angle and wavelength regions of the input light, the FOV of the modified Savart polariscope is still restricted severely.

## 2.2. Combination of two Savart polariscopes

Fig. 5 shows the structure of the presented Savart polariscope. Compared to the previous structures, the developed Savart polariscope is comprised by two conventional Savart polariscopes fabricated from positive and negative birefringent materials respectively.

Employing Eq. (3) in Section 2.1, the OPD given by the described Savart polariscope can be written as

$$\Delta = \Delta_{P1} - \Delta_{P2} + \Delta_{N1} - \Delta_{N2}$$

$$= \left( t_{P} \frac{a_{P}^{2} - b_{P}^{2}}{a_{P}^{2} + b_{P}^{2}} + t_{N} \frac{a_{N}^{2} - b_{N}^{2}}{a_{N}^{2} + b_{N}^{2}} \right) (\cos \omega + \sin \omega) \sin i$$

$$+ \left( t_{P} \frac{a_{P}^{2} - b_{P}^{2}}{(a_{P}^{2} + b_{P}^{2})^{3/2}} \cdot \frac{a_{P}^{2}}{\sqrt{2}} + t_{N} \frac{a_{N}^{2} - b_{N}^{2}}{(a_{N}^{2} + b_{N}^{2})^{3/2}} \cdot \frac{a_{N}^{2}}{\sqrt{2}} \right)$$

$$\times \left( \sin^{2} \omega - \cos^{2} \omega \right) \sin^{2} i,$$
(6)

here the fourth and higher power terms of  $\sin i$  have been neglected for they are too small relative to the quadratic term. The subscript letter P and N in the equation denote the positive and negative uniaxial crystal respectively. From Eq. (6), we can see that the term in  $\sin^2 i$  can be set to be zero when the thicknesses of the two Savart polariscopes are chosen obey the following condition as

$$\frac{t_{P}}{t_{N}} = -\frac{\frac{a_{N}^{2} \left(a_{N}^{2} - b_{N}^{2}\right)}{\left(a_{N}^{2} + b_{N}^{2}\right)^{3/2}}}{\frac{a_{P}^{2} \left(a_{P}^{2} - b_{P}^{2}\right)}{\left(a_{P}^{2} + b_{P}^{2}\right)^{3/2}}} = -\frac{\left(\frac{n_{o} \left(n_{o}^{2} - n_{e}^{2}\right)}{n_{e} \left(n_{o}^{2} + n_{e}^{2}\right)^{3/2}}\right)_{N}}{\left(\frac{n_{o} \left(n_{o}^{2} - n_{e}^{2}\right)}{n_{e} \left(n_{o}^{2} + n_{e}^{2}\right)^{3/2}}\right)_{P}}.$$
(7)

In this way, the straight line fringes can be acquired in a much wider FOV, because only the term in sin *i* is remained in the OPD of the Savart polariscope. Although the coefficient (lateral displacement) of

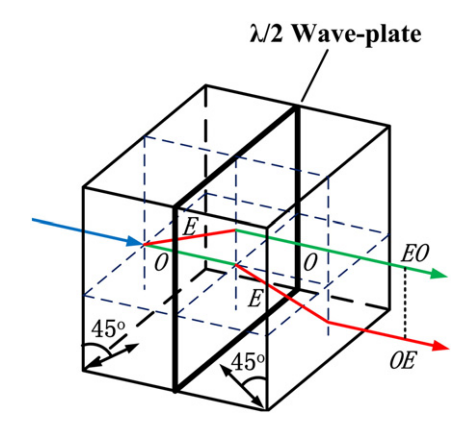
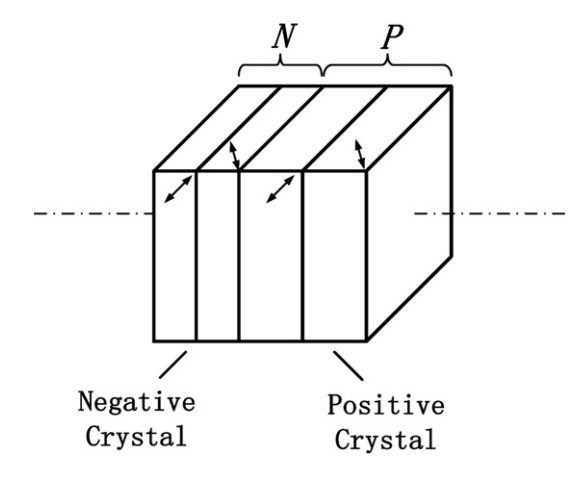


Fig. 4. Modified Savart polariscope presented by Françon.



**Fig. 5.** Novel design of the Savart polariscope described by the present authors.

sin i become smaller, the FOV (sin i) could be remarkably increased. Thus the corresponding OPD can be very large. Note that because of the dispersiveness of the material, the thickness ratio described in Eq. (7) could set the sin  $^2i$  term to be zero only at a single wavelength, but the  $\lambda/2$  condition still holds good in an ultra broadband spectra. Both of these will be demonstrated with a design example in Section 3.

### 3. Analysis and discussion

### 3.1. FOV of a FTS based on Michelson interferometer

For a conventional FTS based on a Michelson interferometer, the condition on the FOV can be defined as [17]

$$i_{\rm M} \approx \sqrt{\frac{2\lambda}{\Delta_{max}}},$$
 (9)

where  $i_M$  is the acceptance incidence angle;  $\lambda$  is the wavelength of the input light;  $\Delta_{\max}$  is the corresponding OPD given by the FTS.

For a Michelson-based FTS, with a maximum OPD of 45  $\mu$ m,  $i_M$  varies from  $\pm 7.64^{\circ}$  at 400 nm to  $\pm 12.67^{\circ}$  at 1100 nm.

### 3.2. FOV of a FTS based on a conventional Savart polariscope

As discussed above, the FTS based on a conventional Savart polariscope has a very limited FOV, because of the distortion in the interferogram caused by the  $\sin^2 i$  term of the OPD. From Eq. (4), its acceptance incidence angle  $i_{CS}$  can be written as

$$i_{\rm CS} \approx \sqrt{\frac{\lambda}{t\sqrt{2}} \cdot \frac{n_e (n_o^2 + n_e^2)^{3/2}}{n_o (n_o^2 - n_e^2)}},$$
 (10)

where  $\lambda$  is the wavelength of the input light, and t is the thickness of a single Savart plate.

For a FTS based on a conventional Savart polariscope made up of two 9-mm-thick calcite plates,  $i_{\rm CS}$  varies from  $\pm\,1.34^\circ$  at 400 nm to  $\pm\,2.33^\circ$  at 1100 nm. The corresponding maximum OPD is from  $\pm\,35\,\mu{\rm m}$  to  $\pm\,54\,\mu{\rm m}$ . Here the refractive indices of the calcite corresponding to the wavelength range from 400 to 1100 nm were calculated using the Sellmeier equation expressed as [18]

$$n_o^2 = 2.69705 + 0.0192064 / \left(\lambda^2 - 0.01820\right) - 0.0151624 \lambda^2, \tag{11a} \label{eq:normalization}$$

$$n_e^2 = 2.18438 + 0.0087309 / (\lambda^2 - 0.01018) - 0.0024411\lambda^2,$$
 (11b)

where the operating wavelength  $\lambda$  is in  $\mu$ m.

Fig. 6 is the calculated FOV interferogram for the FTS based on the conventional Savart polariscope. Where angle  $\alpha$  and  $\beta$  are the projections of the incidence angle i onto the principle sections of the first and second crystal plates of the Savart polariscope, respectively. As described in Section 2.1, the second and higher power terms of  $\sin i$  in Eq. (3) bring the hyperbolic fringes in the margins of the interferogram. Only the central fringe is available and the corresponding FOV can be read out directly. It should be indicated that to make the interferogram clear, only fringes produced by  $\sin^2 i$  are shown.

#### 3.3. FOV of a FTS based on the combination of two Savart polariscopes

As discussed in Section 2.2, the FOV of a Savart polariscope can be increased with the addition of a second Savart polariscope which fabricated from material with opposite signs of birefringence to that of the first one. In order to show the efficiency of this method, a design example operating in 400–1100 nm is proposed.

In the double-polariscope design presented here, as shown in Fig. 5, the first Savart polariscope consists of two 2-mm-thick calcite Savart plates and the second Savart polariscope is fabricated from yttrium vanadate (YVO<sub>4</sub>). YVO<sub>4</sub> is a positive uniaxial crystal for which the refractive indices corresponding to the range 400–1100 nm can be calculated using the Sellmeier equation given as [19]

$$n_o^2 = 3.77834 + 0.069736 / \left(\lambda^2 - 0.04724\right) - 0.0108133\lambda^2, \tag{12a}$$

$$n_e^2 = 4.59905 + 0.110534 / \left( \lambda^2 - 0.04813 \right) - 0.0122676 \lambda^2. \tag{12b} \label{eq:new_energy}$$

Substituting Eqs. (11a) and (12b) into Eq. (7), the optimum thickness of a single crystal plate for the second Savart polariscope  $t_P$  can be obtained. Here we choose  $t_P = 3.52$  mm which is optimized at

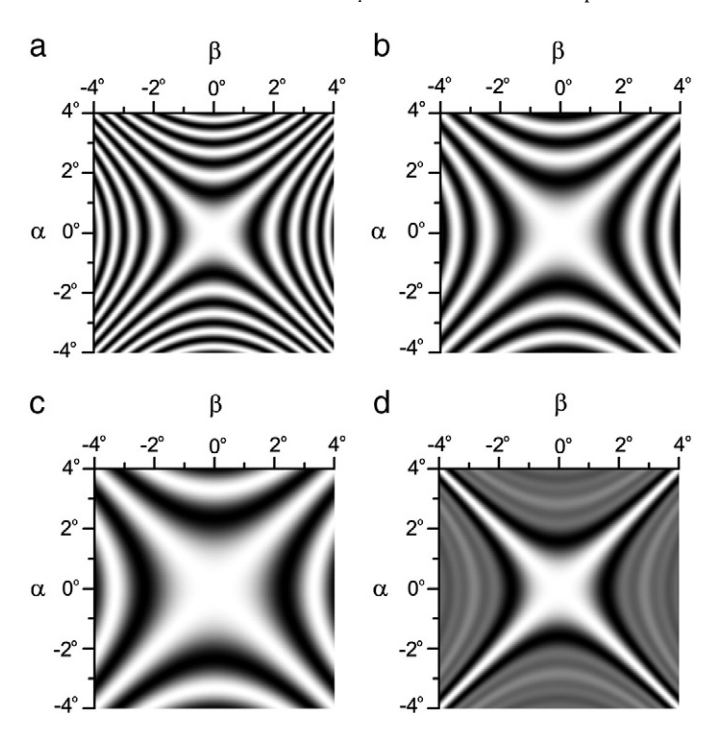


**Fig. 6.** Calculated FOV interferogram for the FTS described in Section 3.2: (a) at 400 nm, (b) at 632.8 nm, (c) at 1100 nm, (d) polychromatic light 400–1100 nm.

the wavelength 632.8 nm. The total thickness of the two Savart polariscopes is only 11.04 mm.

Using a similar  $\lambda/2$  condition as described in Section 2.1, the acceptance incidence angle of the developed FTS  $i_{MS}$  can be written as

$$i_{MS} \approx \arcsin\left(\sqrt{\frac{\lambda}{\sqrt{2}}} \cdot \left| \frac{1}{t_P \left[\frac{n_o \left(n_o^2 - n_e^2\right)}{n_e \left(n_o^2 + n_e^2\right)^{3/2}}\right]_P + t_N \left[\frac{n_o \left(n_o^2 - n_e^2\right)}{n_e \left(n_o^2 + n_e^2\right)^{3/2}}\right]_N} \right|\right).$$
(13)

For the design example described above,  $i_{MS}$  varies from  $\pm$  42.49° at 400 nm to  $\pm 44.67^{\circ}$  at 1100 nm and in a broadband (460–900 nm), the FOV of the developed FTS is only limited by the numerical aperture of the optical components of the FTS. Fig. 7 is the calculated FOV interferogram for the developed FTS. By comparing with Fig. 6, it is observed that the FOV of the developed FTS has been increased much larger than that of the conventional Savart polariscope based FTS. Fig. 8 shows the OPD produced by the developed FTS at 632.8 nm. It can be seen that the OPD of  $\pm$  45 µmis obtained at an incidence angle of  $\pm$  19° at 632.8 nm. In practice, the FOV of the developed FTS can be increased even wider with the combination of two thinner Savart polariscopes. For example with  $t_N = 1$  mm,  $t_P = 1.76$  mm, the FOV of the resulting instrument can be increased to  $\pm 72.78^{\circ}$  at 400 nm and  $\pm 83.85^{\circ}$  at 1100 nm. Its corresponding OPD of  $\pm$  45  $\mu m$  can be obtained at  $\pm$  40° at 632.8 nm. To the best of our knowledge, no previous FTS could have such a large FOV with the similar OPD.

We now consider about the optical efficiency of the input light. For a Michelson-based FTS, half of the light is reflected back to the source and so its maximum optical efficiency is 50%. The developed FTS here may be regarded as a typical birefringent interferometer and hence has a maximum efficiency of 25% for unpolarized light and 50% for a linearly polarized source [7]. With a general consideration of the FOV, input aperture and optical efficiency, optical throughput of the FTS based on the combination of two Savart polariscopes is nearly one order of magnitude higher than that of a conventional Michelson-based FTS.

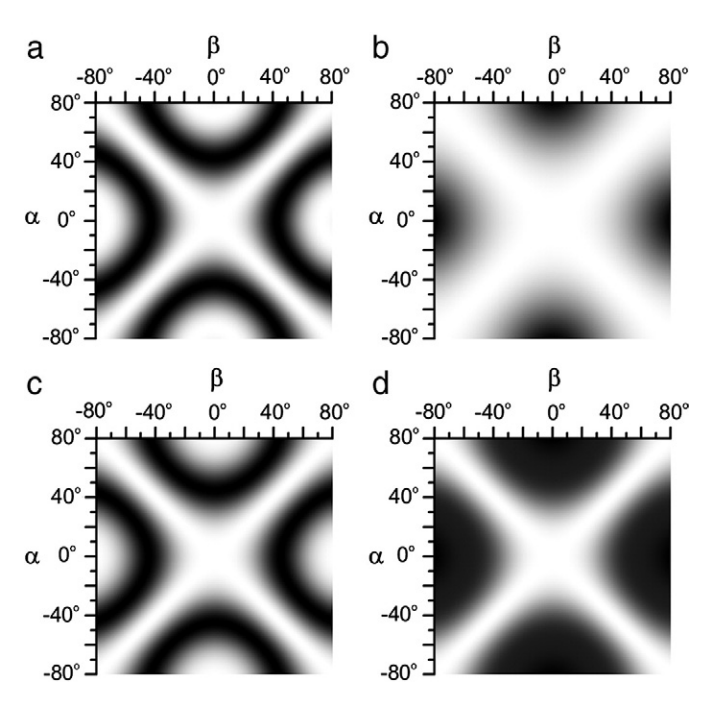


**Fig. 7.** Calculated FOV interferogram for the FTS described in Section 3.3: (a) at 400 nm, (b) at 632.8 nm, (c) at 1100 nm, (d) polychromatic light 400–1100 nm.

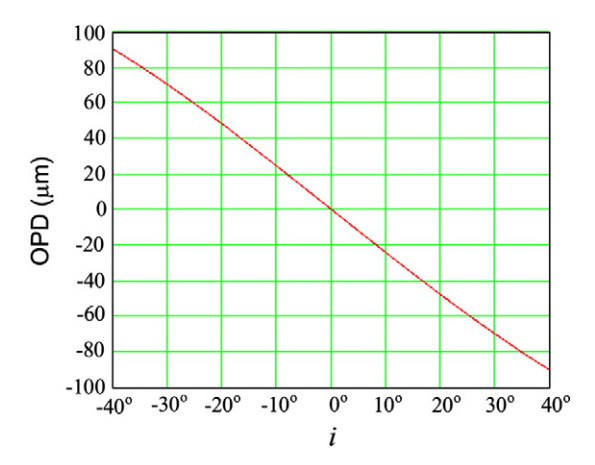


Fig. 8. OPD introduced by the developed FTS at 632.8 nm.

### 4. Conclusion

We have proposed a novel design of a static FTS that combines two Savart polariscopes fabricated from positive and negative birefringent materials. We showed that, with the second compensation Savart polariscope, it can have a much larger FOV that is limited only by the numerical aperture of optical components. Comparing with the conventional FTS based on a Michelson interferometer, the most remarkable advantage of the proposed instrument is a simple, compact, miniature, and static (no moving parts) along with a very large optical throughput. These are important benefits for many practical applications, for example, the fieldwork and space applica-

tions where illumination is weak and the system size and weight are

## Acknowledgement

This work is partially supported by the National High Technology Research and Development Program of China ("863" Program).

### References

- [1] M.J. Persky, Rev. Sci. Instrum. 66 (1995) 4763.
- [2] J.R. Dupuis, M.S. Ünlü, Opt. Lett. 33 (2008) 1368.
- [3] R.J. Bell, Introductory Fourier Transform Spectroscopy, Academic, 1972, p. 22.
- [4] G. Zhan, Appl. Opt. 41 (2002) 560.
- [5] B. Culshaw, Meas. Sci. Technol. 17 (2006) R1.
- [6] M.J. Padgett, A.R. Harvey, Rev. Sci. Instrum. 66 (1995) 2807.
- [7] B.A. Patterson, M. Antoni, J. Courtial, A.J. Duncan, W. Sibbett, M.J. Padgett, Opt. Commun. 130 (1996) 1.
- 8] D. Steers, W. Sibbett, M.J. Padgett, Appl. Opt. 37 (1998) 5777.
- [9] S. Prunet, B. Journet, G. Fortunato, Opt. Eng. 38 (1999) 983.
- [10] M. Hashimoto, S. Kawata, Appl. Opt. 31 (1992) 6096.
- [11] K. Tsukino, T. Satoh, H. Ishii, M. Nakata, Chem. Phy. Lett. 457 (2008) 444.
- [12] J. Courtial, B.A. Patterson, A.R. Harvey, W. Sibbett, M.J. Padgett, Appl. Opt. 35 (1996) 6698.
- [13] G. Boer, T. Scharf, R. Dändliker, Appl. Opt. 41 (2002) 1400.
- 14] M. Françon, S. Mallick, Polarization Interferometers: Applications in Microscopy and Macroscopy, Wiley-Interscience, 1971, p. 24.
- [15] C. Zhang, T. Mu, W. Ren, L. Zhang, N. Liu, Opt. Eng. 49 (2010) 043002.
- [16] M. Françon, S. Mallick, Polarization Interferometers: Applications in Microscopy and Macroscopy, Wiley-Interscience, 1971, p. 144.
- [17] R.J. Bell, Introductory Fourier Transform Spectroscopy, Academic, 1972, p. 149.
- [18] "Calcite Crystal," Casix, http://www.casix.com/product/prod\_cry\_calcite.html.
- [19] "Yttrium Vanadate (YVO<sub>4</sub>) Crystal," Casix, http://www.casix.com/product/ prod\_cry\_yvo4.html.